Journal of Hydrology 641 (2024) 131841

Contents lists available at ScienceDirect

Journal of Hydrology

journal homepage: www.elsevier.com/locate/jhydrol

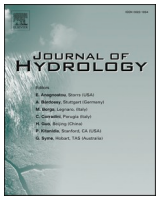

Research papers

The patterns of potential evapotranspiration and seasonal aridity under the change in climate in the upper Blue Nile basin, Ethiopia

Gashaw Gismu Chakilu [a,b,*], Szegedi Sándor [c], Túri Zoltán [d], Kwanele Phinzi [e]

[a] Doctoral School of Earth Sciences, University of Debrecen, Egyetem tér 1, Debrecen 4032, Hungary
[b] Department of Natural Resources Management, Debark University, Debark, Ethiopia
[c] Department of Meteorology, University of Debrecen, Egyetem tér 1, Debrecen 4032, Hungary
[d] Department of Physical Geography and Geoinformatics, University of Debrecen, Egyetem tér 1, Debrecen 4032, Hungary
[e] Department of Geography and Environmental Studies, University of Zululand, KwaDlangezwa, 3886, South Africa

ARTICLE INFO

This manuscript was handled by Sally Elizabeth Thompson, Editor-in-Chief, with the assistance of Tara Troy, Associate Editor

Keywords:
Climate change
Potential evapotranspiration
Aridity index
Upper blue nile
Ethiopia

ABSTRACT

Evapotranspiration is one of the determinant components of the hydrological process, highly influenced by climate change due to the increase in atmospheric temperature at global and regional scales. This study was designed to evaluate the extent to which climate change affects the Potential Evapotranspiration (PET) and the consequent Aridity Index (AI) in the high-emission scenario of Representative Concentration Pathways (RCPs) in the Gilgel Abay, Ribb, Gumara, and Megech watersheds using six Global Climate Models in the 2011–2040, 2041–2070, and 2071–2100 relative to the 1971–2000 (baseline period). The average PET is simulated using the Soil Water Assessment Tool (SWAT) model. Penman-Monteith and Hargreaves methods were used in the computation of PET using the water balance technique, and the Hargreaves method was found more efficient in calibration and validation processes. The Aridity Index (AI) of watersheds is calculated using the ratio of precipitation and potential evapotranspiration. The study revealed that the change in annual average PET is showing an increasing pattern in the three time periods, and the highest rate of changes in Megech, Gilgel Abay, Ribb, and Gumara, watersheds are 16.66%, 15.53%, 14.68%, and 13.46%, respectively in the 2071–2100 time period. Seasonally, the highest rate of change in PET is 20.37% (September), 19.29% (April), 17.46% (March), and 17.02% (March) in the Megech, Gilgel Abay, Ribb, and Gumara, respectively. Similarly, the seasonal highest change in Aridity Index (AI) is also likely to be observed in the 2071–2100 in which in the dry season, it accounts –0.303 (March), –0.299 (March), –0.285 (April), and –0.276 (April) in the Ribb, Gumara, Gilgel Abay, and Megech, respectively, whereas in the rainy season, the change is 0.263, 0.258, 0.238, and 0.211 in the Gilgel Abay, Gumara, Ribb, and Megech, respectively. In general, due to the rising atmospheric temperature, the amount of moisture during dry seasons in the headwater catchments of the upper Blue Nile basin is expected to deplete in the 21st century. Therefore, it is highly recommended to use different climate change adaptation mechanisms including adopting suitable physical and biological water conservation techniques to enhance the amount of water stored in the subsurface and joining the groundwater during the rainy season.

1. Introduction

Climate change is currently one of the most important global problems, disturbing the societal socio-economic, and environmental situations (Fulco et al, 2007). The impact of climate change becomes more visible in water resources, affecting the distribution and allocation in spatial and temporal aspects globally, making water scarcity a very serious global problem (Sun et al., 2008). The larger responsible driving factors for the change in climate at global and regional levels are anthropogenic activities, resulting in the emission of Greenhouse Gases (GHGs) (Henderson & Reinert, 2016). The future climate change is projected based on the possible continuing greenhouse gas emissions, land use change, and air pollutant emissions in the 21st century (IPCC, 2014).

Evapotranspiration (ET) is one of the important components of the hydrological cycle which can potentially be altered by climate change.

* Corresponding author at: Doctoral School of Earth Sciences, Department of Meteorology, University of Debrecen, Egyetem tér 1, Debrecen 4032, Hungary.
E-mail addresses: gashaw.gismu@dku.edu.et (G. Gismu Chakilu), szegedi.sandor@science.unideb.hu (S. Sándor), turi.zoltan@science.unideb.hu (T. Zoltán), phinzik@unizulu.ac.za (K. Phinzi).

https://doi.org/10.1016/j.jhydrol.2024.131841
Received 14 October 2022; Received in revised form 10 July 2024; Accepted 6 August 2024
Available online 15 August 2024

The term represents the combination of the two words evaporation and transpiration. The former implies the process by which water is moving directly from the land surface (soil, water bodies, and canopies) to the air, whereas the latter refers to the movement of water from the soil, through roots and vegetation bodies, on leaves, and then into the air. Potential Evapotranspiration (PET) is the maximum amount of water that can be lost by evapotranspiration if sufficient water is available, influenced by temperature, humidity, sunlight, and wind (Allen et al., 1998). The assessment of the PET or reference evapotranspiration (ETo) is very important for various hydro-climatic applications including designing and management of irrigation projects, water balance studies, and assessment of droughts and aridity index classification (Wang & Dickinson, 2012) (McMahon et al., 2013) (Weiß & Menzel, 2008). In recent years, it is well verified that climate change has become a major driving factor for the loss of water through evapotranspiration (Qu & Zhuang, 2019) (G. G. Haile & Tang, 2020) and increasing aridity on regional and global scales.

Aridity is a climatic phenomenon that refers to the long-term persisting climatic condition over a region (Agnew, 1991), expressed in terms of the Aridity Index which is defined by the ratio of total annual precipitation to potential evapotranspiration (Huang et al., 2016). Even though the changes in temperature and precipitation are considered as the two main indicators of climate change, AI is more important to understand the change in climate in terms of the bioclimatic condition (Moral et al., 2017). Due to the consistent rising temperature and declining water availability, it is indicated that aridity will increase over the 21st century in different parts of the world (Marvel et al., 2019) (Park et al., 2018) (Lin et al., 2018) (Fu et al., 2016) (Dai, 2013). Thus, it significantly alters the natural and human systems (Corlett, 2020), and once the aridity or dryness of a particular region increases beyond a certain level, it will be very tough to restore it (Adnan & Haider, 2012).

Though it is well known that climate change is significantly affecting global water availability (IPCC, 2022a), regionally, the distinct impacts of climate change on evapotranspiration should be quantified and projected to assess the dynamics of moisture availability. This consideration will enhance our understanding of its impact on water resources and ecosystem services in general (Allen et al., 2011) in large river basins and small-scale catchments. Numerous researches have revealed that climate change has been affecting the evapotranspiration condition of river basins in tropical regions. For instance, the rate of change in evapotranspiration is expected to rise by up to 4.8 % in the Tapajós Basin in the Brazilian Amazon (Farinosi et al., 2019), 12.7 % in the Subarnarekha basin in tropical India under RCP 8.5 scenario. In the Ethiopian context, the availability of water is projected to be prominently altered by climate change through the loss of much water by the evapotranspiration process in the upper Blue Nile basin (A. T. Haile et al., 2017) (Taye et al., 2018), Tekeze basin (Gebremeskel & Kebede, 2018), and Gilgel Gibe basin (Alemayehu et al., 2023).

Most importantly, the rate of change in PET and rainfall under the change in climate in the upper Blue Nile basin is well studied and the overall results showed that there is a consistent increment of PET in various watersheds, whereas, the rate of change in rainfall is highly fluctuating in temporal and spatial patterns under different emission scenarios (G. G. Chakilu et al., 2020) (Worqlul et al., 2018) (Kim & Kaluarachchi, 2009) (G. G. Chakilu et al., 2023). According to (Mengistu et al., 2021), PET is expected to increase up to 27 % by the end of the 21st century under the RCP 8.5 scenario, whereas, rainfall is likely to decline up to 19 % under the same scenario in the upper Blue Nile basin. On the other hand, a study by (G. G. Chakilu et al., 2022a) indicated that the rate of change in rainfall is projected to rise up to 27 % in the rainy season and decrease up to 19 % in the dry season at the end of 21st century in the same basin and under the same emission scenario. Similarly, (Bekele et al., 2021) reported that rainfall is expected to decline by up to 21 %, and rise in PET by up to 7 % in the mid-21st century under the RCP 8.5 scenario.

The result of all the above studies clearly showed the consistent rise of PET due to increasing temperature, and seasonal fluctuation of rainfall with a decline in the dry season. Most of these results are used to evaluate the impact of climate change on stream flow of watersheds in the Upper Blue Nile basin. However, the consequent impact of the consistent and long-term increase of PET on the declining land moisture availability, or level of seasonal aridity in the entire area of watersheds especially in the dry season, has not been investigated in the basin. Thus, the objectives of this study are: 1) to assess the rate of change in precipitation (rainfall); 2) to evaluate the rate of change in potential evapotranspiration; and 3) to calculate the level of seasonal aridity or dryness in terms of Aridity Index (AI) in the headwater catchments of the Upper Blue Nile basin. For this investigation, the study focused on using the RCP8.5 scenario because the projected temperature and the subsequent PET in global and regional contexts are rising prominently under this scenario compared to other RCPs. Hence, it is always good to consider the worst-case scenario in the investigation for planning watershed development and management practices and applying different climate change adaptation and resilience mechanisms in the basin. However, the authors suggested that researchers should consider the Shared Socio-Economic Pathway (SSP5-8.5) in CMIP6 climate models in similar future studies because the degree of increase in temperature and PET under this pathway is higher than RCP8.5.

2. Methods and materials

2.1. Study area description

This study was conducted in the headwater catchments of the upper Blue Nile basin, Ethiopia namely: Megech, Gilgel Abay, Ribb, and Gumara watersheds (Fig. 1). The investigated watersheds are the subwatersheds of the Lake Tana sub-basin which is the head and major source of the Blue Nile basin, geographically located between 10.95° and 12.78° N and 36.89° and 38.25° E. More than 93 % of water of the Lake Tana which is the largest lake in Ethiopia is collected from these four watersheds (Setegn, 2010). The general geophysical characteristics of the watersheds are presented in Table 1.

2.2. Hydro-climate data processing

Climate variables that are mainly used in this study are rainfall, maximum temperature (T_{max}), and minimum temperature (T_{min}). These climate variables with different spanning periods were obtained from Ethiopia's National Meteorological Agency (NMA). Even though, there are more stations in the region, only 14 meteorological stations were considered in the investigated watersheds because of lack of sufficient years of data (Table 2). Due to this, some of the stations were commonly used for two adjacent watersheds in the simulation process. Stations which are having a better spanning period of observed data were used for the bias correction process of projected climate variables and evaluation of the efficiency of investigated climate models. The missing values of climate variables were replaced by the average values of data of the nearest weather stations on the corresponding date (Te Chow et al., 1988) for bias correction purposes. However, for the period, used for the SWAT model were replaced by the model itself.

Six climate models including CSIRO-Mk3-6–0, HadGEM2-ES, EC-EARTH, CanESM2, NORESM1-M, and CNRM-CM5 were used in climate data projection under the Coupled Model Inter-comparison Project Phase 5 (CMIP5) (Table 3). Earth System Grid Federation (ESGF) was used as a data source, accessed at https://esgf-node.llnl.gov/projects/esgf-llnl/ website. Except for HadGEM2-ES, the other five climate models were selected based on their Equilibrium Climate Sensitivity (ECS) values which are within the recommended range value (1.5 to 4.5 °C) in CMIP5 (Meehl et al., 2020) (Wyser et al., 2020), whereas HadGEM2-ES was selected because of its good performance in the projection of surface temperature and precipitation in other previous studies (Kattsov et al., 2013) (Bhattacharjee & Zaitchik, 2015).

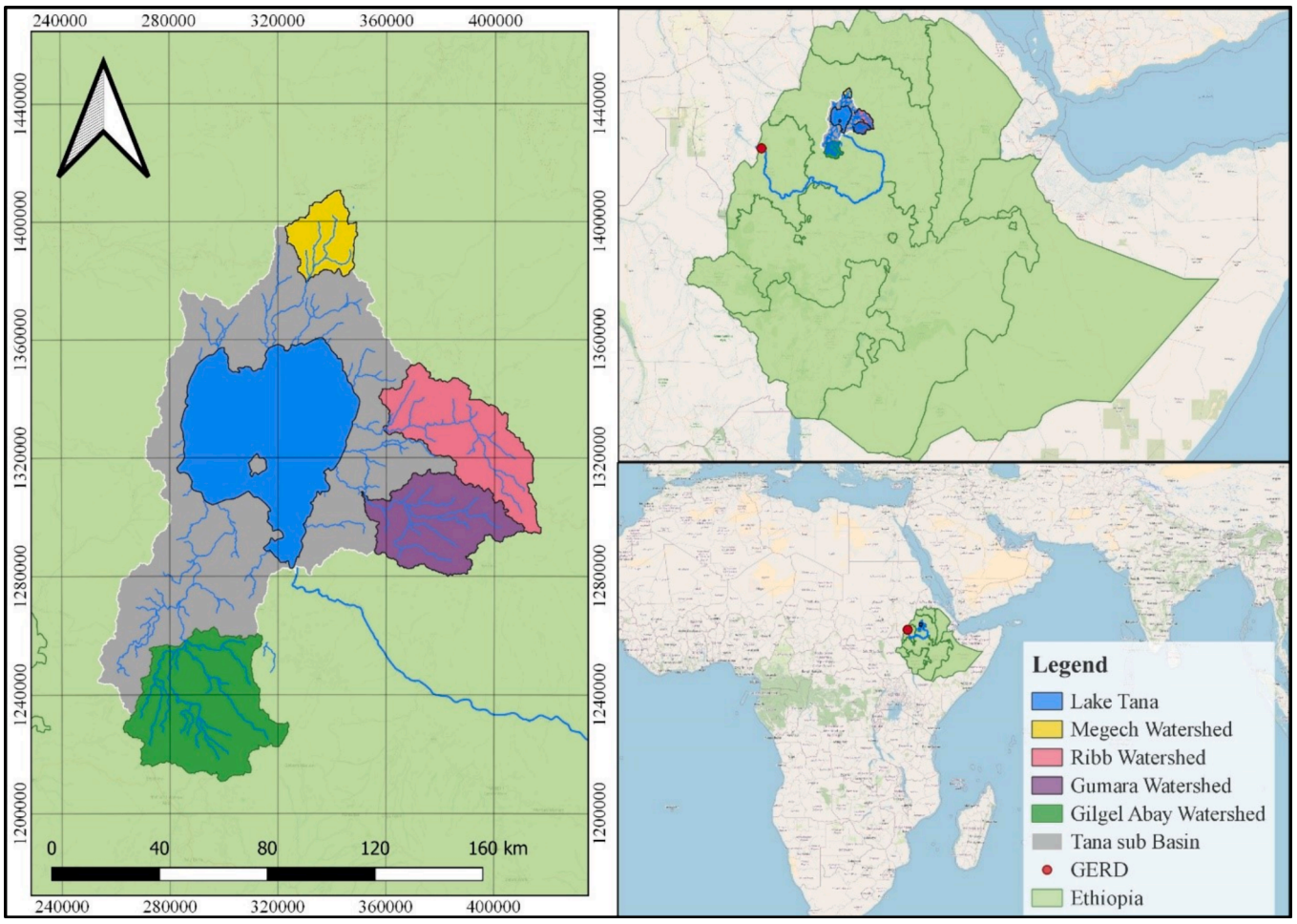

Fig. 1. Location map of the study area.

The raw observed streamflow data of watersheds was obtained from the MoWE and processed before being used in the SWAT model simulation.

2.3. Geophysical data collection and processing

The geophysical data such as soil, land use/cover, and slope were required to define and analyze of Hydrological Response Unit (HRU) in the simulation process of streamflow in the SWAT model. Soil data was obtained from the global digital soil map (FAO-UNESCO, 2007) with a 1:5000000 scale, whereas the land use was taken from Ethiopian MoWE. The slope of watersheds was generated from SRTM Digital Elevation Model (DEM) data with 30 m*30 m resolution, accessed from the United States Geological Survey (USGS). These geospatial data were processed using ArcGIS10.4 software based on the compatibility of the SWAT model.

2.4. Correction of errors in climate model outputs

The projected future climate data were corrected using the historical 30 years (1971–2000) of observed and model output data of climate variables. Mostly, the biases between the projected and observed climate data are created because of the spatial resolution factors of climate models and topographical differences. Therefore, minimizing the great variation and maintaining the consistency and reliability of the future projected time series data is highly important for climate change analysis and impact studies. For this purpose, various statistical methods are being applied especially in future rainfall and temperature projections in various climate studies. In this study, the power transformation method was used for the correction of errors in rainfall climate model outputs, whereas both the T_{max} and T_{min} model outputs were corrected by the variance scaling method using CMhyd software (Rathjens et al., 2016). These two bias correction methods are selected based on the level of consistency of results in frequency-based statistics in previous studies (Teutschbein & Seibert, 2012) (Fang et al., 2015). Therefore, the amount of rainfall R in each day is transformed into a corrected R* by using Equation (1) as follows:

$$R^* = aR^b \tag{1}$$

The value of "a" and "b" are determined iteratively.

The corrected daily temperature (T_{corr}) for both T_{max} and T_{min} was obtained by using Equation (2):

$$T_{corr} = \overline{T}_{obs} + \frac{\sigma(T_{obs})}{\sigma(T_{gcm})}\left(T_{gcm} - \overline{T}_{gcm}\right) \tag{2}$$

Where T_{gcm} is the uncorrected daily projected historical T_{max} and T_{min}; T_{obs} stands for observed daily T_{max} and T_{min}; the symbols "σ" and "¯" represent the mean and standard deviation of values, respectively.

2.5. Estimation of potential evapotranspiration

The PET of watersheds is simulated by the Soil Water Assessment Tool (SWAT) model using energy balance and temperature-based methods. Even though there are many PET estimation methods, the SWAT model supports only three methods. In the temperature-based

Table 1
The geophysical characteristics of investigated watersheds.

Watersheds	Area (Km^2)	Altitude (m.a.s.l.)	Major soil types	Major land uses
Gilgel Abay	1754	1385–3584	– Haplic Luvisols (55.1 %) – Haplic Alisols (37.8 %)	– Agriculture (72.78 %) – Agro-pastoral (23.54 %)
Ribb	1407	1793–4112	– Eutric Leptosols (39.8 %) – Chromic Luvisols (35.1 %) – Eutric Fluvisols (24.7 %)	– Agriculture (60.25 %) – Agro-pastoral (23.05 %) – Pastoral (16.44 %)
Gumara	1272	1797–3712	– Haplic Luvisols (63.7 %) – Chromic Luvisols (24.3 %) – Eutric Leptosols (9 %)	– Agriculture (63.31 %) – Agro-pastoral (31.24 %) – Pastoral (5 %)
Megech	514	1848–2972	– Eutric Leptosols (80.1 %) – Haplic Nitisols (9 %) – Chromic Luvisols (6 %)	Agriculture (%)

The soil data of watersheds was obtained from the global digital soil map (FAO-UNESCO, 2007), whereas the land use was taken from the Ethiopian Ministry of Water and Energy (MoWE). The land uses and soil types with less than 5% area coverage of the watersheds are not included in the study area description (Table 1).

Table 2
The meteorological stations with their geographical location and altitude.

Stations	Latitude (degree)	Longitude (degree)	Altitude (meter)
Injibara	10.99	36.92	2568
Bahir Dar	11.60	37.36	1800
Wetet Abay	11.37	37.04	1920
Adet	11.27	37.49	2179
Dangila	12.25	36.84	2125
Sekela	10.98	37.21	2715
Wanzaye	11.78	37.67	1821
Debretabor	11.86	37.99	2612
Werota	11.92	37.69	1819
Ageregenet	11.80	38.29	3010
Amedber	11.91	37.88	1141
Addis Zemen	12.12	37.77	1940
Gondar	12.3	37.25	1973
Makisegnit	12.39	37.55	1912

Table 3
The investigated global climate models with their Equilibrium Climate Sensitivity (ECS) and resolution.

Climate model	ECS	Resolution (Lat x Lon)
CSIRO-Mk3-6–0	4.37 °C	1.875°x1.875°
HadGEM2-ES	4.64 °C	1.875°x1.25°
EC-EARTH	3.3 °C	1.125°x1.125°
CanESM2	3.7 °C	2.81°x2.81°
NORESM1-M	2.8 °C	1.9°x2.5°
CNRM-CM5	3.3 °C	1.4°x1.4°

method, only the Hargreaves method is used, whereas in the energy balance method, Penman-Monteith and Priestley Tylor estimation methods are supported in the SWAT model. Therefore, for this study, Penman-Monteith which is commonly used in the energy balance method was used in this study, whereas, in the temperature–based method, Hargreaves method was used in the PET simulation process. The result of these two methods was compared based on their performance in the simulation of stream flow by the SWAT model, and the best-fit method was selected and used in change analysis in PET and aridity index. PET in the Penman-Monteith method is calculated by equation (3).

$$ET_O = \frac{0.408\Delta(R_n - G) + \gamma \frac{900}{T+273} u_2 (e_s - e_a)}{\Delta + \gamma(1 + 0.34u_2)} \quad (3)$$

Where ETo = reference evapotranspiration (mm/day); Δ= slope of the vapor pressure curve (kPa/°C); γ = psychrometric constant (kPa/°C); Rn = net radiation at the crop surface ($MJ/m^2/d$); G=soil heat flux density ($MJ/m^2/d$); T=mean daily air temperature at 2 m height (°C); u_2 = wind speed at 2 m height (m/s); e_s = saturation vapor pressure (kPa); e_a = actual vapor pressure (kPa); e_s–e_a = saturation vapor pressure deficit (kPa). The net radiation (Rn) is calculated by the following formula equation (4).

$$R_n = \left((1 - albo)\left(0.25 + 0.5\frac{n}{N}\right)R_a\right) - \left(0.9\frac{n}{N} + 0.1\right)(0.34 - 0.14\sqrt{e_d})\sigma(T + 273.2)^4 \quad (4)$$

Where albo = albedo, a measure of surface reflectivity; n = sunshine hours per day (h); N=total length of the day (h); Ra = extraterrestrial radiation ($MJ/m^2/day$); e_d = vapor pressure (kPa); σ = Stefan-Boltzmann constant ($4.903*10^{-9} MJ\ m^{-2o} K^{-4}\ day^{-1}$); T=mean air temperature (°C).

The study area does not have adequate meteorological stations, and even the existing stations have not long-term meteorology data, most importantly stations have limitations in providing data for some climate variables like humidity, solar radiation, and wind speed. The weather generator was developed using Climate Forecast System Reanalysis (CFSR) climate data for the region with the required format of the SWAT model (Dile & Srinivasan, 2014). Even though the applicability of CFSR climate data for hydrological models has already been verified, it has some uncertainty and errors compared to the ground-based data. Due to this, PET has also been estimated using Hargreaves, or a temperature-based method that mainly uses T_{max} and T_{min}. In this method, PET is calculated using equation (5):

$$PET = 0.0023 R_a (T_{max} - T_{min})^{0.5} \left(\frac{T_{max} + T_{min}}{2} + 17.8\right) \quad (5)$$

R_a is also computed using equation (6):

$$R_a = 15.392 d_r (w_s \sin f \sin d + \cos f \cos d \sin w_s) \quad (6)$$

Where d_r is the relative distance between the earth and sun; w_s is the sunset hour angle (radians); f is the latitude of a site (+for Northern Hemisphere, − for Southern Hemisphere) (radians); d is the solar declination (radians); and J is Julian day.

$$d_r = 1 + 0.033\cos\left(\frac{2\pi J}{365}\right) \quad (7)$$

$$w_s = arccos(-\tan f \tan d) \quad (8)$$

$$d = 0.4093\sin\left(\frac{2\pi J}{365} - 1.405\right) \quad (9)$$

2.6. Validation of simulated potential evapotranspiration

Though the estimated value of PET should be verified by ground-measured data, in the region, it is difficult to get measured lysimetric data. Therefore, in this study, the verification is done by evaluating the performance in the simulation of streamflow of watersheds. In the validation process, the SWAT model considers PET as one of the important water balance components, and if the simulated streamflow is

consistent with the measured flow, it is assumed that the estimated PET is also consistent with reality. Thus, in this study, the main purpose of using the SWAT model is to associate the estimated PET with the simulated streamflow of watersheds. The SWAT model uses a water balance algorithm in the simulation process using equation (10) (Neitsch et al., 2002).

$$SW_t = SW_0 + \sum_{i=1}^{t} \left(R_{day} - Q_{surf} - E_a - W_{sweep} - Q_{gw}\right)_i \quad (10)$$

Where SW_t = the final soil water content (mm), Q_{surf} = the amount of surface runoff (mm), i = time step (day), t = is time (days), SW_o = the initial soil water content (mm), R_{day} = the amount of precipitation (mm), W_{seep} = the amount of water entering the vadose zone from the soil profile (mm), E_a = the amount of evapotranspiration (mm), and Q_{gw} = the amount of groundwater flow (mm).

2.7. Calibration and validation of the SWAT model

The simulated flow, obtained by the default parameters and values of parameters was compared with the measured one, and a great difference was observed. To minimize this deviation, the sensitive SWAT model parameters were selected and calibrated using SWAT-CUP (SWAT-Calibration and Uncertainty Programs) version 12 software. The model was calibrated by seven years (1995–2001) of climate data in the four watersheds and the efficiency of the model was evaluated. The maximum efficiency of the model was observed after 2000 iterations through automatic calibration and by manual adjustment of parameter values. Once the maximum efficiency of the model and the optimum values of parameters were obtained, the consistency was also verified by four years (2002–2005) of climate data. Since the purpose of the study is to investigate climate change impacts, the same geophysical inputs of the SWAT model are used in the calibration and validation process. The efficiency of the SWAT model in default simulation, calibration, and validation was evaluated by using two statistical variables including Nash–Sutcliffe (NS), and Relative Volume Error (RVE), computed by equation (11) and equation (12), respectively.

$$NS = 1 - \frac{\sum_{i=1}^{n}\left(Q_{sim(i)} - Q_{obs(i)}\right)^2}{\sum_{i=1}^{n}\left(Q_{sim(i)} - \overline{Q}_{obs}\right)^2} \quad (11)$$

Where Q_{obs} is the daily observed streamflow and Q_{sim} also represents the daily simulated streamflow, n = the number of days. The value of NS ranges between $-\infty$ and 1; 1 indicates the best performance of the model (Nash & Sutcliffe, 1970).

$$RVE = \frac{\sum_{i=1}^{n}\left(Q_{obs(i)} - Q_{sim(i)}\right)}{\sum_{i=1}^{n} Q_{obs(i)}} * 100\% \quad (12)$$

The optimal value of RVE is 0, whereas, the positive and negative values indicated underestimation and overestimation of the model, respectively (Gupta et al., 1999).

2.8. Estimation of aridity Index (AI)

AI is the level of dryness of a certain region, expressed numerically. It is an index that indicates the availability of moisture in the soil, defined as the ratio between mean annual precipitation (P) and mean annual PET (UNEP, 1993).

$$AI = \frac{P}{PET} \quad (13)$$

Even though AI is usually estimated based on the mean annual precipitation and PET, this study evaluated it based on the seasonal variability of precipitation and PET to assess the seasonal aridity condition of the region. Therefore, first, the change in precipitation and PET were evaluated in the mean monthly time scale, and the aridity index was also estimated accordingly.

3. Results and discussion

3.1. Evaluation of the performance of climate models

The performance of each model has been evaluated by comparing the simulated data with the corresponding station-observed data. The errors of climate models in the simulation of T_{max}, T_{min}, and rainfall are analyzed in terms of monthly time scale. Compared to the other climate models, the CanESM2 was the least efficient in the projection of all climate variables. All climate models have better efficiency in the simulation of T_{min} than T_{max}. The highest average monthly errors of climate models in the simulation of historical rainfall, T_{max}, and T_{min} ranged from ± 0.85 % to ± 1.17 %, 0.12 °C to 0.19 °C, and 0.08 °C to 0.14 °C, respectively (Fig. 2). All the highest variations in the three climate variables are observed in the CanESM2, whereas the lowest errors in the projection of both rainfall and T_{min} are detected by the CSIRO-Mk3-6–0 and in T_{max}, it is under NORESM1-M model. These errors in all climate variables under all climate models are evaluated after the bias correction process is completed. Therefore, these errors could be considered as one of the causes for uncertainties observed in the simulation of PET and have an impact on the overall efficiency of the SWAT model Fig. 3..

3.2. SWAT model efficiency

SWAT model was more efficient in simulating stream flow using the Hargreaves PET estimation method than the Penman-Monteith (PM) method in all watersheds, which is consistent with other comparison studies (Earls & Dixon, 2008) (Oudin et al., 2005) (Almorox et al., 2015). In both PET estimation methods, the best fit was observed in the Gilgel Abay watershed compared to the others in calibration and verification processes interms of NS (HR=0.86, PM=0.79). In the Megech watershed, although the performance of the model is improved by calibration, it is still weak compared to the other watersheds. Statistically, the performance of the model (NS) using the HR PET estimation method was 0.51 and 0.54 in the calibration and verification process, respectively, whereas in the PM method, the model performance in terms of NS was 0.47 and 0.56 in the calibration and verification process, respectively. The efficiency of the SWAT model in terms of RVE was also evaluated and the result showed that PET estimation using the HR method was more appropriate than PM in almost all watersheds, except

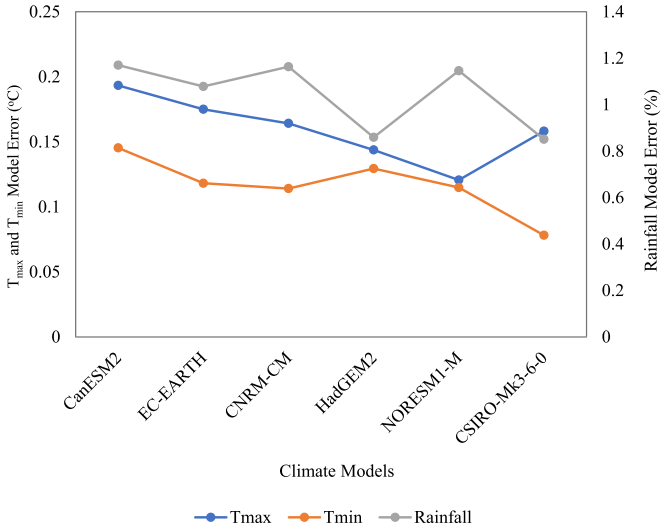

Fig. 2. Climate model errors in the simulation of T_{max}, T_{min}, and Rainfall.

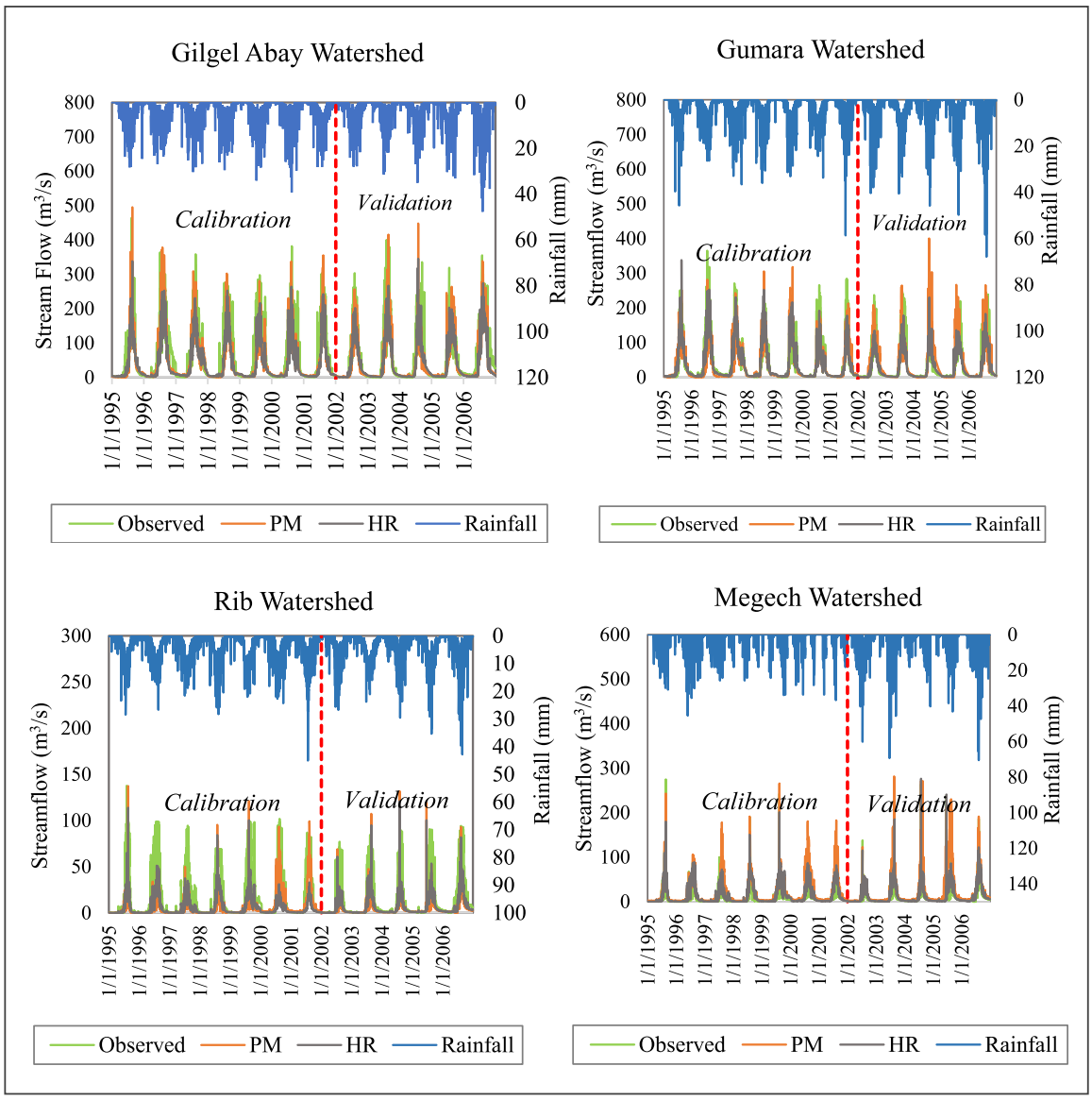

Fig. 3. Observed flow Vs simulated flow of watersheds using PM and HR methods.

in the model validation period of the Megech watershed (HR=–6.62 % and PM=–4.6 %). The negative values of RVE in the default simulation, calibration, and validation process indicated that there is an over-estimation of streamflow (Table 4).

The optimal values of sensitive parameters obtained by the calibration process were tested again by independent climate data for verification purposes, and it was found that the performance of the model was consistent in the validation process as well. The rank of the sensitivity of parameters was evaluated based on the *t*-test and p-values. A parameter with the highest *t*-test value regardless of its sign, and the lowest p-value has the highest degree of sensitivity (Table 5).

The model was more efficient in the PM method than HR in capturing the peak flows in almost all watersheds, though there were over-estimations in some calibration and verification years, especially in the Megech watershed. On the other hand, the HR method is more consistent in the low flow of watersheds.

3.3. Change in rainfall

The ensemble mean values of rainfall data obtained from the six climate models were taken as input for the SWAT model and the mean value in each watershed was computed by the Thiessen polygon method.

Table 4
Comparison of the Penman-Monteith and Hargreaves methods in SWAT model performance.

Watersheds	Default performance				Calibration				Verification			
	NS		RVE (%)		NS		RVE (%)		NS		RVE (%)	
	HR	PM	HR	PM	HR	PM	HR	PM	HR	PM	HR	PM
Gilgel Abay	0.15	0.07	32.41	41.37	0.86	0.79	1.31	4.62	0.84	0.75	1.36	1.95
Gumara	0.18	0.11	36.84	39.83	0.67	0.63	1.25	3.86	0.63	0.52	1.88	2.73
Ribb	0.09	0.02	28.69	32.46	0.71	0.68	1.14	2.94	0.74	0.81	1.07	3.84
Megech	−0.32	−0.4	−48.52	−34.6	0.51	0.47	−8.84	11.32	0.54	0.56	−6.62	−4.6

Table 5
SWAT model parameters with their range, fitted value, and rank of sensitivity.

Watershed	Parameter	t-stat	P-value	Min Value	Max value	Fitted value	Rank
	R_CN2.mgt	−10.14	0	0	1	0.14	1
	V_ALPHA_BF.gw	5.48	0	−25	25	−12	2
	V_ESCO.hru	−3.07	0.03	0	1	0.42	3
	V_GW_DELAY.gw	−2.9	0.09	0	10	7.34	4
	V_GW_REVAP.gw	−2.23	0.11	0.02	0.2	0.19	5
	R_CN2.mgt	−58	0	−0.2	0.2	−0.18	1
	V_ALPHA_BF.gw	10.8	0	0	1	0.12	2
	A_SOL_K.sol	6.1	0	−0.5	1	0.47	3
	V_GW_REVAP.gw	−1.2	0.2	0.02	0.2	0.10	4
	V_GWQMN.gw	1	0.3	0	10	1.31	5
	V_ESCO.hru	3.76	0.01	0	1	0.5	1
	R_SOL_AWC.sol	3.55	0.01	0	1	0.9	2
	V_EPCO.hru	2.55	0.04	0	1	0.7	3
	R_CN2.mgt	−1.95	0.09	−0.2	0.2	2.37	4
	V_ALPHA_BF.gw	1.77	0.12	0	1	0.5	5
	R_CN2.mgt	−10.55	0.00	−0.2	0.2	−0.02	1
	V_ALPHA_BF.gw	−8.27	0.00	0	1	0.76	2
	V_GW_DELAY.gw	−2.70	0.01	0	10	5.37	3
	V_GWQMN.gw	2.26	0.03	0	2	0.55	4
	A_SOL_K.sol	1.90	0.06	−0.5	1	−0.17	5

The change in rainfall in an annual time scale of all periods is evaluated compared to the baseline period (1971–2000). The change in rainfall in all watersheds and all periods ranges from 2.59 % to 4.87 %. The highest change is expected in the last thirty period of this century (2071–2100) in the Gumara watershed. Since the watersheds shared common meteorology stations the change in rainfall in the three periods showed the same pattern except for Megech watershed which showed a little decrement between the second (2041–2070) and the last period (2071–2100). Therefore, it is possible to conclude that in all periods, the mean annual rainfall showed an increasing trend in almost all watersheds (Fig. 4).

In the study area, rainfall is common in the summer season (June – September), in the other seasons especially in the winter season, the area is dry. Therefore, the study was also committed to revealing the variability of changes seasonally in terms of monthly time scale. In all watersheds, the change in rainfall is showing an increasing trend in the summer and post–summer (autumn) seasons. Whereas, in the winter and spring seasons in almost all watersheds and periods, rainfall is expected to decrease compared to the baseline period. The change is more prominent in November in the Gumara, Ribb, and Megech watersheds; while in the Gilgel Abay watershed, it is higher in October. The highest increasing values of the change in the Gumara, Megech, Ribb, and Gilgel Abay watersheds are 19.69 % (November), 18.56 % (November), 16.09 % (November), and 14.80 % (October) in the 2041–2070, 2041–2070, 2071–2100, and 2071–2100 periods, respectively. The highest decreasing values of the change in Gilgel Abay, Megech, and Gumara watersheds are expected to be observed in March, and the values of changes are 7.74 %, 5.66 %, and 5.53 %, respectively in 2071–2100, but in the Ribb watershed, it is likely to be observed in June, and the magnitude of the change is 4.63 % in 2041–2070 (Fig. 5).

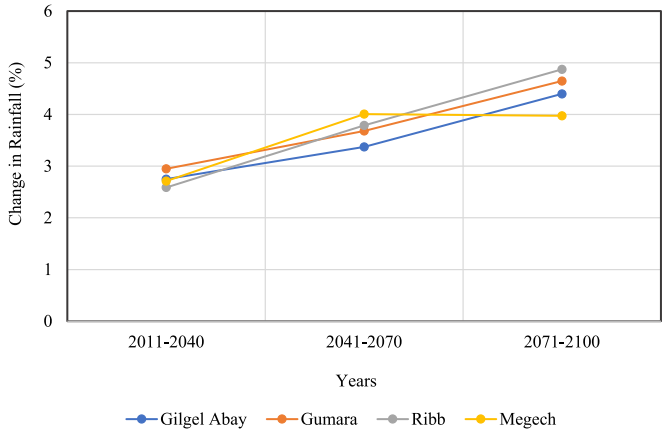

Fig. 4. Change in annual rainfall in Gilgel Abay, Gumara, Ribb, and Megech watersheds.

3.4. Change in potential evapotranspiration (PET) of watersheds

The Potential Evapotranspiration (PET) of all watersheds was computed by the Penman-Monteith and Hargreaves method in the calibration and verification process of the SWAT model, and the result was compared based on selecting the best fit in streamflow simulation. The change in PET ranges from 5.99% to 16.66% in all watersheds and periods. The change is showing an increasing pattern in all watersheds and in the three time periods, more prominently it showed a significant increment in 2071–2100. In general, the results of this study revealed that the highest change in annual average PET in Megech, Gilgel Abay, Ribb, and Gumara watersheds are 16.66%, 15.53%, 14.68%, and 13.46%, respectively, which is going to be observed in 2071–2100 (Fig. 6).

Like the change in rainfall, the change in PET in the four watersheds and three time periods is also evaluated regarding seasonal variability. As far as PET is computed using the temperature-based (Hargreaves) method, the change is highly based on temperature change, and the pattern of PET change in all watersheds is almost the same due to the watersheds shared common meteorological station in the SWAT model. In Megech and Gilgel Abay watersheds, the highest change in PET is expected to be observed in September and April, respectively, whereas in Gumara and Ribb watersheds, the highest change is more likely observed in March. The highest values of changes in the Megech, Gilgel Abay, Ribb, and Gumara watersheds are 21.17 %, 19.29 %, 19.26 %, and 17.51 %, respectively (Fig. 7). Unlike rainfall, the change in PET in all watersheds, all months, and the three time periods showed an increasing pattern; all values of changes are above zero. Comparatively, the change is more significant in 2071–2100 than in the other periods.

3.5. Change in aridity Index

As shown in sections 2.3 and 2.4, rainfall and PET in the study area showed considerable changes in all watersheds and all periods. Thus, as far as those two important climate variables determine the Aridity Index, the change in Aridity in the four watersheds has also shown an increasing pattern in the coming eight decades of this century. Annually, the change in the Aridity Index is expected to increase within the range

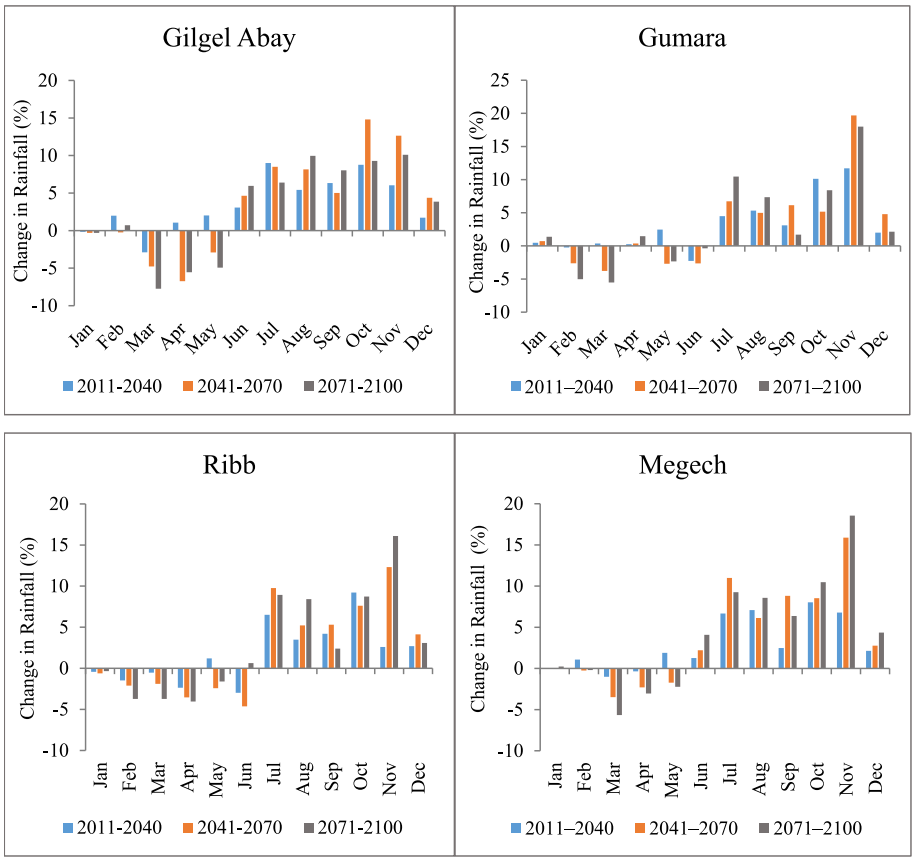

Fig. 5. Change in monthly rainfall in Gilgel Abay, Gumara, Ribb, and Megech watersheds.

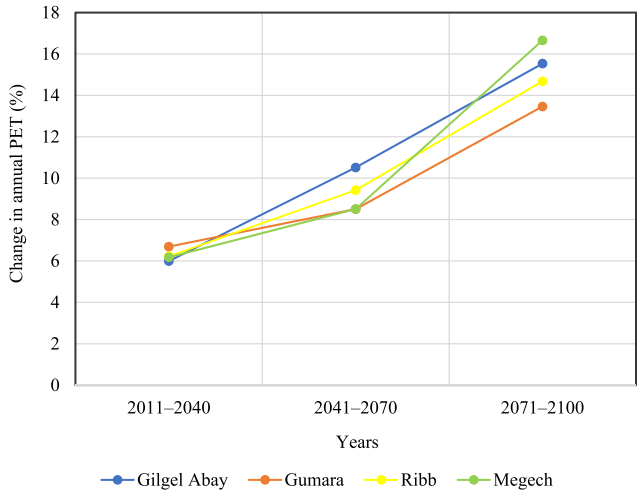

Fig. 6. Change in annual PET in Gilgel Abay, Gumara, Ribb, and Megech watersheds.

of 0.006 to 0.061 in all watersheds and periods. The highest change is forecasted in the 2071–2100 time period in the Megech watershed, while the lowest change is in 2011–2040 in the Gilgel Abay watershed. The negative values of changes in (Fig. 8) indicated that the change in AI is increasing in the region due to the change in temperature and the consequent result of increasing loss of moisture by evapotranspiration. Not only compared to the baseline period, changes between three consecutive periods have shown considerable variability in all watersheds.

Even though by definition Aridity Index is the ratio of annual rainfall and PET, this study intends to evaluate the expected seasonal aridity of the watersheds on a monthly time scale. The dynamics of change in the Aridity Index on a monthly time scale showed increasing and decreasing patterns in all periods and watersheds. The severity of aridity shows a significant increment in the winter season considering the three time periods. Like, the change in PET, the change in AI is more prominent in the last thirty years of this century (2071–2100). In the summer season, the study showed that the area is expected to be wetter than the baseline period. Thus, it indicated that the change in the availability of moisture (rainfall amount) is higher than the loss of moisture because of evapotranspiration in the region. The highest seasonal changes in AI during the winter season in Ribb, Gumara, Gilgel Abay, and Megech watersheds are –0.301 (March), –0.299 (March), –0.285 (April), and –0.273 (April), respectively. On the contrary, during the summer season, the highest changes in the watersheds are observed in August except in the Megech watershed which is observed in July, and the values of changes are 0.263, 0.258, 0.238, and 0.211, respectively (Fig. 9). The negative and positive values of changes in these different seasons indicated that the aridity is increasing and decreasing, respectively.

4. Discussion

The change in rainfall in the Lake Tana sub-basin of the Blue Nile basin does not show a consistent pattern in terms of inter-annual and annual changes. The seasonal fluctuation of the change in rainfall in the region has also been indicated by other similar previous studies (Kim et al., 2008) (Elshamy et al., 2009) (Takele et al., 2022). The increasing rate of change in precipitation in the wet season and decrease in the dry season has directly been causing flooding and drought problems. In general, the change in precipitation could lead to significant and varied shifts in phenology (Huxman et al., 2004) (Cleland et al., 2007), reservoir management (Chaves et al., 2023) (Yasarer & Sturm, 2016), and

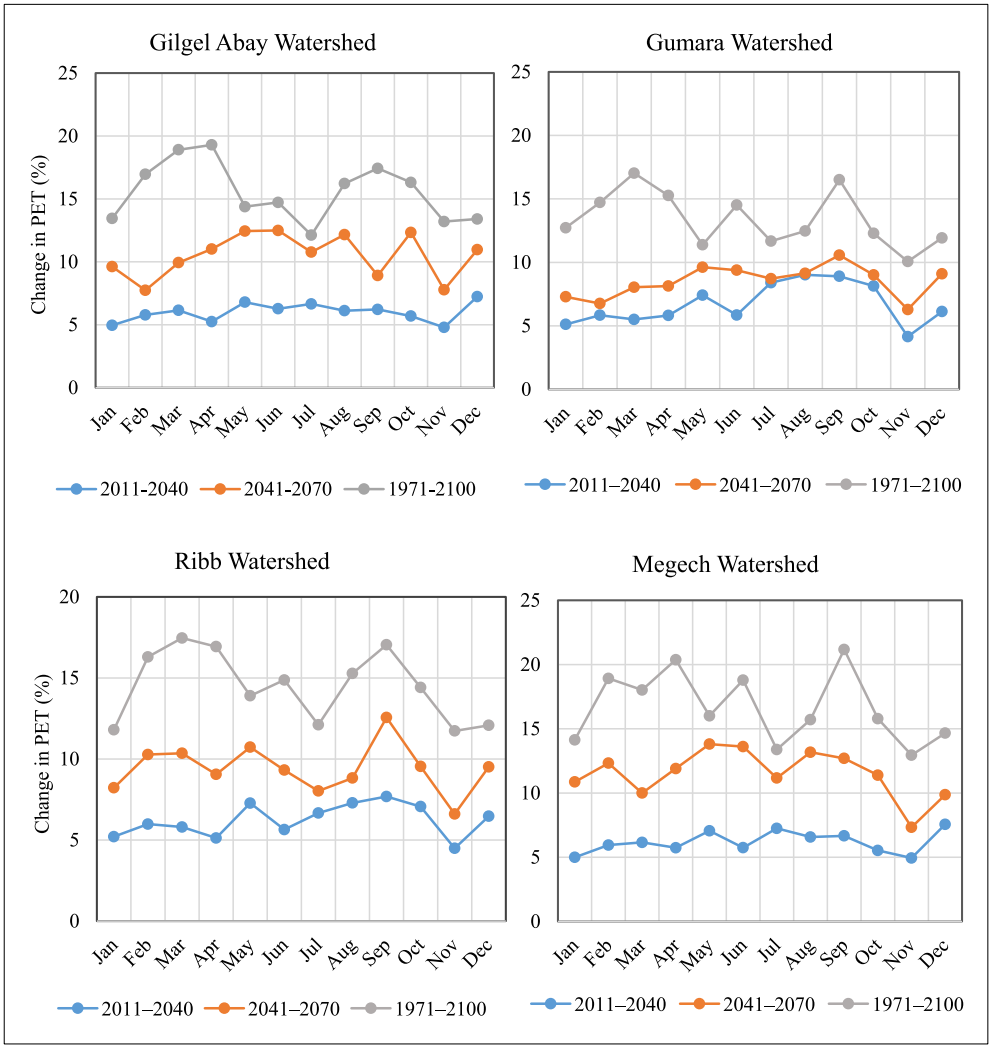

Fig. 7. Seasonal variabilities of the change in PET in Gilgel Abay, Gumara, Ribb, and Megech watersheds.

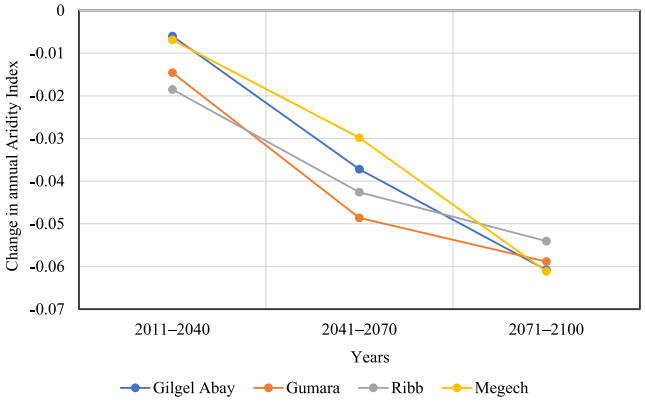

Fig. 8. Change in Aridity Index in Gilgel Abay, Gumara, Ribb, and Megech watersheds.

ecosystem services (Parmesan et al., 2022).

The change in temperature and its impact on the potential evapotranspiration in the upper Blue Nile basin has also been revealed by many other studies including (G. G. Chakilu et al., 2022b) (Ayele et al., 2016) (G. G. Chakilu et al., 2020) and (A. T. Haile et al., 2017), in which the overall results indicated that the rising of atmospheric temperature could significantly cause the increasing of potential evapotranspiration in 21st century under the high emission scenario. For instance, temperature is expected to rise by 4 °C and the rate of change of rainfall shows a decline of 15 % in the dry season and a rise of 15 % in the wet season under RCP 8.5 over the long-term time windows. Similarly, the study conducted by (Takele et al., 2022) showed a temperature rise, and the annual evapotranspiration increased by about 10.4 % in the basin. In the same region, but out of the basin, a comparable trend of rising temperature and the consequent increase of PET is also expected to be observed at the end of this century. For instance, it is projected to increase up to 49.42 % in the Wabe Shebele basin (Gurara et al., 2021) and 22.66 % in the Gilgel Gibe basin (Alemayehu et al., 2023) under the same emission scenario. As PET increases, more water is evaporated from the soil surface and transpired by vegetation, which can lead to increase water demand from natural ecosystems, agriculture, and human settlements. If the increase in PET exceeds the available water supply, leading to water stress, faster soil moisture depletion and affects plant growth, reduced streamflow, and decreased water availability for irrigation, drinking water, and industrial use (Goyal, 2004) (Maracchi et al., 2005).

Even though the investigated study area does not have an aridity problem on an annual basis, the area is going to be highly vulnerable in the dry season due to the sharp rise in temperature and ET. Because the dimensionless values of the Aridity Indexes were estimated using the ratio of rainfall and PET (UNEP, 1993), the increasing change in AI indicated that the water availability of the watersheds is likely to

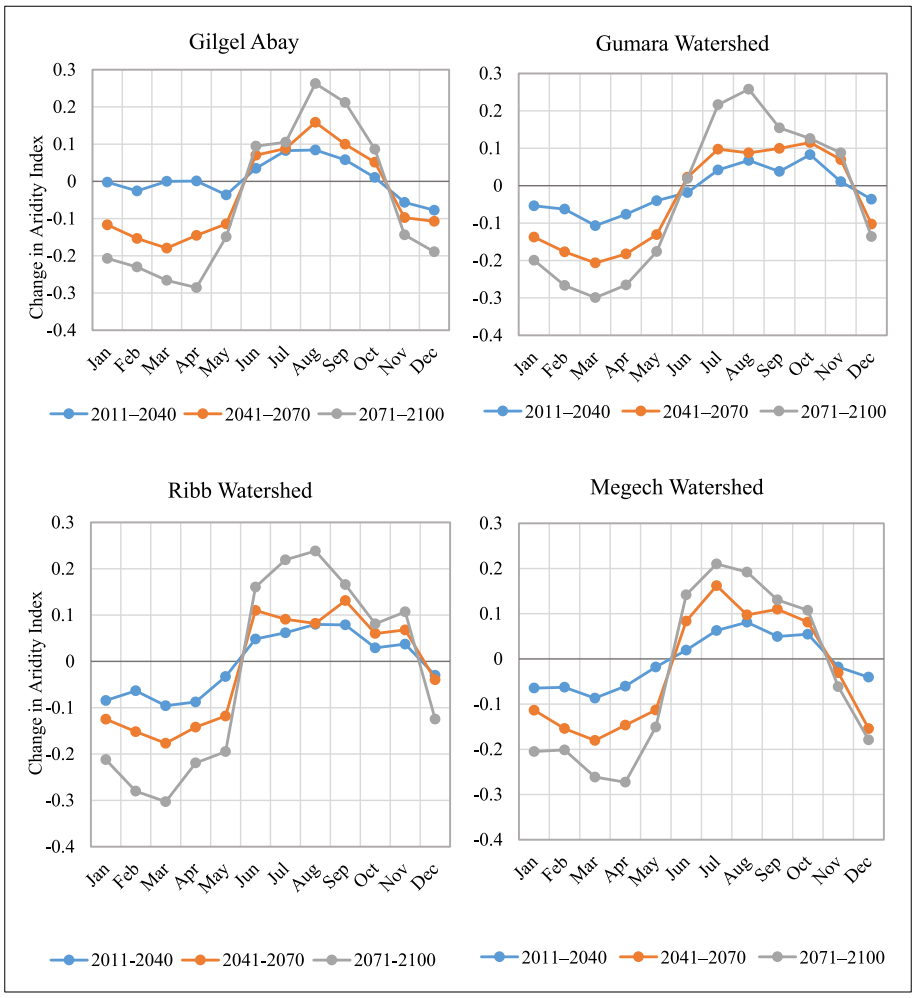

Fig. 9. Change in seasonal Aridity Index in the watersheds.

improve in the region; whereas the decrease in AI implied that the availability of water in the catchments is expected to deplete and leading to water stress in the region. Therefore, the result clearly showed that the dryness of the region is likely to increase in the dry season because of the consistent rise in temperature.

The headwater catchments of the Upper Blue Nile basin are highly degraded due to the expansion of agriculture and the distraction of forest resources (Chakilu & Moges, 2017). Therefore, to minimize the vulnerability of catchments to climate change impacts and, most importantly to minimize the seasonal dryness of the area, it is highly recommended to use different climate change adaptation mechanisms including adopting suitable physical and biological water conservation techniques (Mena, 2018) to enhance the amount of water stored in the subsurface and joining the groundwater in the rainy season.

5. Conclusion

- This study revealed that the change in climate under the high emission (RCP 8.5) scenario has considerably affected the evapotranspiration nature of watersheds in the headwater catchments of the upper Blue Nile basin and consequently, the aridity is expected to increase, especially in the dry season.
- The inter-annual rate of changes in rainfall showed considerable decreasing and increasing patterns in the dry and wet seasons, respectively, whereas the annual average rate of change is not likely to be significant in all watersheds.
- The projected rise in temperature is going to be directly affecting the water resources of watersheds in a way that escalates the evaporation of moisture from the soil, and transpiration from plants.
- The projected change in PET in the four watersheds is anticipated to increase consistently in both seasonal and annual time scales in all periods with a prominent rise in the 2071–2100 under the ensemble mean of all climate models.
- This study has also evaluated how much the ratio of rainfall and PET, i.e., Aridity Index (AI)) in all catchments is expected to change in the three consecutive periods. Due to the fluctuation of the change in rainfall, the change in AI does not show significant dynamics on an annual average basis, unlike PET. Seasonally, the variability of changes in AI is high between dry and wet seasons. In the dry season, due to an increment in temperature, and decreasing in rainfall, the change in aridity shows a significant increasing pattern, whereas in the wet season, even though there is an increment of PET, an increment of moisture availability because of rainfall is much higher than the loss of moisture by PET, aridity is decreasing.
- Generally, the result indicated that in the dry season, the region is likely to be drier, and in wet seasons it is predicted to be wetter in all watersheds and the three time periods especially in the 2071–2100.
- The overall results of the study give important indications on the potential impacts of climate change on the overall health of ecosystems in the headwater catchments of the upper Blue Nile basin and the consequent effects on natural and human systems due to the declining water availability in the lower catchment communities including in Egypt and Sudan.

Author Contributions

G.G.C. collected, processed, and analyzed climate, hydrological, and geophysical data; and writing of the paper. S.S. and T.Z. followed up on the whole work, and K.P. also contributed his role in an edition of the paper.

CRediT authorship contribution statement

Gashaw Gismu Chakilu: Writing – review & editing, Writing – original draft, Software, Methodology, Investigation, Formal analysis, Data curation, Conceptualization. **Szegedi Sándor:** Supervision. **Túri Zoltán:** Supervision. **Kwanele Phinzi:** Writing – review & editing.

Declaration of competing interest

The authors declare that they have no known competing financial interests or personal relationships that could have appeared to influence the work reported in this paper.

Data availability

The data that has been used is confidential.

Acknowledgments

A special is given to the two Ethiopian organizations (NMA and MoWE) where the meteorological, hydrological, and geophysical data are obtained.

References

Adnan, S., & Haider, S. (2012). Classification and assessment of aridity in Pakistan by using different aridity indices ftp://ftp. wmo. int/Documents/PublicWeb/arep/Weather_Mod_Bali/ENV% 20bruntjes. chalon. *ENV. Adnan_Pakistan_paper1. Pdf. Accessed, 21*.

Agnew, C.T., 1991. Disaster in the arid realm. Choices and Environments. Collins Educational, London, Societies, pp. 56–79.

Alemayehu, Z., Id, T., Bizuneh, Y. K., & Mekonnen, A. G. (2023). *The impacts of climate change on hydrological processes of Gilgel Gibe catchment , southwest Ethiopia*. 1–28. DOI: 10.1371/journal.pone.0287314.

Allen, R.G., Pereira, L.S., Raes, D., Smith, M., 1998. Crop evapotranspiration-Guidelines for computing crop water requirements-FAO Irrigation and drainage paper 56. Fao, Rome 300 (9), D05109.

Allen, R.G., Pereira, L.S., Howell, T.A., Jensen, M.E., 2011. Evapotranspiration information reporting: I. Factors governing measurement accuracy. Agric Water Manag 98 (6), 899–920.

Almorox, J., Quej, V.H., Martí, P., 2015. Global performance ranking of temperature-based approaches for evapotranspiration estimation considering Köppen climate classes. J. Hydrol. 528, 514–522.

Ayele, H.S., Li, M.H., Tung, C.P., Liu, T.M., 2016. Impact of climate change on runoff in the Gilgel Abbay watershed, the upper Blue Nile Basin, Ethiopia. Water (switzerland) 8 (9). https://doi.org/10.3390/w8090380.

Bekele, W.T., Haile, A.T., Rientjes, T., 2021. Impact of climate change on the streamflow of the Arjo-Didessa catchment under RCP scenarios. J. Water Clim. Change 12 (6), 2325–2337.

Bhattacharjee, P.S., Zaitchik, B.F., 2015. Perspectives on CMIP5 model performance in the Nile. River. 4275 (February), 4262–4275. https://doi.org/10.1002/joc.4284.

Chakilu, G., Moges, M., 2017. Assessing the land use/cover dynamics and its impact on the low flow of Gumara Watershed, Upper Blue Nile Basin. Ethiopia. *Hydrol Current Res* 7 (2).

Chakilu, G.G., Sándor, S., Zoltán, T., 2020. Change in stream flow of gumara watershed, upper blue nile basin, ethiopia under representative concentration pathway climate change scenarios. Water (switzerland) 12 (11), 1–14. https://doi.org/10.3390/w12113046.

Chakilu, G.G., Sándor, S., Zoltán, T., Phinzi, K., 2022a. Climate change and the response of streamflow of watersheds under the high emission scenario in Lake Tana sub-basin, upper Blue Nile basin, Ethiopia. J. Hydrol.: Reg. Stud. 42 (March) https://doi.org/10.1016/j.ejrh.2022.101175.

Chakilu, G.G., Sándor, S., Zoltán, T., Phinzi, K., 2022b. Climate change and the response of streamflow of watersheds under the high emission scenario in Lake Tana sub-basin, upper Blue Nile basin. Ethiopia. *Journal of Hydrology: Regional Studies* 42, 101175.

Chakilu, G.G., Sándor, S., Zoltán, T., 2023. The Dynamics of Hydrological Extremes under the Highest Emission Climate Change Scenario in the Headwater Catchments of the Upper Blue Nile Basin. Ethiopia. 1–21.

Chaves, H.M.L., da Silva, C.C., Fonseca, M.R.S., 2023. Reservoir Reliability as Affected by Climate Change and Strategies for Adaptation. Water (switzerland) 15 (13). https://doi.org/10.3390/w15132323.

Cleland, E.E., Chuine, I., Menzel, A., Mooney, H.A., Schwartz, M.D., 2007. Shifting plant phenology in response to global change. Trends Ecol. Evol. 22 (7), 357–365. https://doi.org/10.1016/j.tree.2007.04.003.

Corlett, R.T., 2020. The impacts of climate change in the Tropics. Clim. Change 84–85. https://doi.org/10.4000/books.irdeditions.34319.

Dai, A., 2013. Increasing drought under global warming in observations and models. Nat. Clim. Chang. 3 (1), 52–58.

Dile, Y.T., Srinivasan, R., 2014. Evaluation of CFSR climate data for hydrologic prediction in data-scarce watersheds: An application in the blue nile river basin. J. Am. Water Resour. Assoc. 50 (5), 1226–1241. https://doi.org/10.1111/jawr.12182.

Earls, J., Dixon, B., 2008. A Comparison of SWAT Model-Predicted Potential Evapotranspiration Using Real and Modeled Meteorological Data. Vadose Zone J. 7 (2), 570–580. https://doi.org/10.2136/vzj2007.0012.

Elshamy, M.E., Seierstad, I.A., Sorteberg, A., 2009. Impacts of climate change on Blue Nile flows using bias-corrected GCM scenarios. Hydrol. Earth Syst. Sci. 13 (5), 551–565.

Fang, G.H., Yang, J., Chen, Y.N., Zammit, C., 2015. Comparing bias correction methods in downscaling meteorological variables for a hydrologic impact study in an arid area in China. Hydrol. Earth Syst. Sci. 19 (6), 2547–2559. https://doi.org/10.5194/hess-19-2547-2015.

FAO-UNESCO. (2007). *Digit al Soil Map of t he World*. 2007.

Farinosi, F., Arias, M. E., Lee, E., & Longo, M. (2019). *Future Climate and Land Use Change Impacts on River Flows in the Tapajós Basin in the Brazilian Amazon Earth ' s Future*. 993–1017. DOI: 10.1029/2019EF001198.

Fu, Q., Lin, L., Huang, J., Feng, S., Gettelman, A., 2016. Changes in terrestrial aridity for the period 850–2080 from the Community Earth System Model. J. Geophys. Res. Atmos. 121 (6), 2857–2873.

Gebremeskel, G., Kebede, A., 2018. Estimating the effect of climate change on water resources: Integrated use of climate and hydrological models in the Werii watershed of the Tekeze river basin. Northern Ethiopia. *Agriculture and Natural Resources* 52 (2), 195–207. https://doi.org/10.1016/j.anres.2018.06.010.

Goyal, R.K., 2004. Sensitivity of evapotranspiration to global warming: a case study of arid zone of Rajasthan (India). Agric Water Manag 69 (1), 1–11.

Gupta, H.V., Sorooshian, S., Yapo, P.O., 1999. Status of automatic calibration for hydrologic models: Comparison with multilevel expert calibration. J. Hydrol. Eng. 4 (2), 135–143.

Gurara, M.A., Jilo, N.B., Tolche, A.D., 2021. Impact of climate change on potential evapotranspiration and crop water requirement in Upper Wabe Bridge watershed, Wabe Shebele River Basin. Ethiopia. *Journal of African Earth Sciences* 180, 104223.

Haile, A.T., Akawka, A.L., Berhanu, B., Rientjes, T., 2017. Changes in water availability in the Upper Blue Nile basin under the representative concentration pathways scenario. Hydrol. Sci. J. 62 (13), 2139–2149. https://doi.org/10.1080/02626667.2017.1365149.

Haile, G. G., & Tang, Q. (2020). *Projected Impacts of Climate Change on Drought Patterns Over East Africa Earth ' s Future*. 1–23. DOI: 10.1029/2020EF001502.

Henderson, P. R. M., & Reinert, S. A. (2016). *P O L I N a D E K H T Y a R a M R a M M I G D a L. Mba 2016*. www.hbsp.harvard.edu.

Huang, J., Yu, H., Guan, X., Wang, G., Guo, R., 2016. Accelerated dryland expansion under climate change. Nat. Clim. Chang. 6 (2), 166–171.

Huxman, T.E., Snyder, K.A., Tissue, D., Leffler, A.J., Ogle, K., Pockman, W.T., Sandquist, D.R., Potts, D.L., Schwinning, S., 2004. Precipitation pulses and carbon fluxes in semiarid and arid ecosystems. Oecologia 141 (2), 254–268. https://doi.org/10.1007/s00442-004-1682-4.

IPCC. (2014). Intergovernmental p Panel on Climate Change: Sythesis Report. In *Managing the Risks of Extreme Events and Disasters to Advance Climate Change Adaptation: Special Report of the Intergovernmental Panel on Climate Change* (Vol. 9781107025). DOI: 10.1017/CBO9781139177245.003.

IPCC. (2022a). *Future Climate Changes , Risks and Impacts Box 2 . 1 Advances , confidence and uncertainty in modelling the Earth ' s climate system Box 2 . 2 The Representative Concentration Pathways (RCPs)*. *1*, 1–23.

Kattsov, V., Federation, R., Reason, C., Africa, S., Uk, A. A., Uk, T. A., Baehr, J., Uk, A. B., Catto, J., Canada, J. S., & Uk, A. S. (2013). *Evaluation of Climate Models 9*.

Kim, U., & Kaluarachchi, J. J. (2009). Climate change impacts on water resources in the upper Blue Nile River Basin, Ethiopia. In *Journal of the American Water Resources Association* (Vol. 45, Issue 6). DOI: 10.1111/j.1752-1688.2009.00369.x.

Kim, U., Kaluarachchi, J. J., & Smakhtin, V. U. (2008). *Climate change impacts on hydrology and water resources of the Upper Blue Nile River Basin, Ethiopia* (Vol. 126). Iwmi.

Lin, L., Gettelman, A., Fu, Q., Xu, Y., 2018. Simulated differences in 21st century aridity due to different scenarios of greenhouse gases and aerosols. Clim. Change 146 (3), 407–422.

Maracchi, G., Sirotenko, O., Bindi, M., 2005. Impacts of present and future climate variability on agriculture and forestry in the temperate regions: Europe. Clim. Change 70 (1–2), 117–135.

Marvel, K., Cook, B.I., Bonfils, C.J.W., Durack, P.J., Smerdon, J.E., Williams, A.P., 2019. Twentieth-century hydroclimate changes consistent with human influence. Nature 569 (7754), 59–65.

McMahon, T.A., Peel, M.C., Lowe, L., Srikanthan, R., McVicar, T.R., 2013. Estimating actual, potential, reference crop and pan evaporation using standard meteorological data: a pragmatic synthesis. Hydrol. Earth Syst. Sci. 17 (4), 1331–1363.

Meehl, G.A., Senior, C.A., Eyring, V., Flato, G., Lamarque, J.F., Stouffer, R.J., Taylor, K. E., Schlund, M., 2020. Context for interpreting equilibrium climate sensitivity and

transient climate response from the CMIP6 Earth system models. Sci. Adv. 6 (26), 1–10. https://doi.org/10.1126/sciadv.aba1981.
Mena, M.M., 2018. Community Adoption of Watershed Management Practices at Kindo Didaye District, Southern Ethiopia. *International Journal of Environmental Sciences & Natural.* Resources 14 (2). https://doi.org/10.19080/ijesnr.2018.14.555881.
Mengistu, D., Bewket, W., Dosio, A., Panitz, H.J., 2021. Climate change impacts on water resources in the Upper Blue Nile (Abay) River Basin. Ethiopia. *Journal of Hydrology* 592, 125614. https://doi.org/10.1016/j.jhydrol.2020.125614.
Moral, F.J., Paniagua, L.L., Rebollo, F.J., García-Martín, A., 2017. Spatial analysis of the annual and seasonal aridity trends in Extremadura, southwestern Spain. Theor. Appl. Climatol. 130 (3), 917–932.
Nash, J.E., Sutcliffe, J.V., 1970. River flow forecasting through conceptual models part I—A discussion of principles. J. Hydrol. 10 (3), 282–290.
Neitsch, S.L., Arnold, J.G., Kiniry, J.R., Srinivasan, R., Williams, J.R., 2002. Soil and Water Assessment Tool User's Manual. TWRI Report TR- 192, 412. http://swat.tamu.edu/media/1294/swatuserman.pdf.
Oudin, L., Hervieu, F., Michel, C., Perrin, C., Andréassian, V., Anctil, F., Loumagne, C., 2005. Which potential evapotranspiration input for a lumped rainfall–runoff model?: Part 2—Towards a simple and efficient potential evapotranspiration model for rainfall–runoff modelling. J. Hydrol. 303 (1–4), 290–306.
Park, C.-E., Jeong, S.-J., Joshi, M., Osborn, T.J., Ho, C.-H., Piao, S., Chen, D., Liu, J., Yang, H., Park, H., 2018. Keeping global warming within 1.5 C constrains emergence of aridification. Nat. Clim. Chang. 8 (1), 70–74.
Parmesan, C., Morecroft, M. D., Trisurat, Y., & Change, C. (2022). *Vulnerability Climate Change 2022 : Impacts , Adaptation and Vulnerability Working Group II Contribution to the Sixth Assessment Report of the Intergovernmental Panel on Climate Change*.
Qu, Y., & Zhuang, Q. (2019). *Evapotranspiration in North America : implications for water resources in a changing climate*.
Rathjens, H., Bieger, K., Srinivasan, R., & Arnold, J. G. (2016). *CMhyd User Manual Documentation for preparing simulated climate change data for hydrologic impact studies*. p.16p.
Setegn, S.G., 2010. Modelling hydrological and hydrodynamic processes in lake Tana basin. Ethiopia, KTH.
Sun, G., McNulty, S.G., Moore Myers, J.A., Cohen, E.C., 2008. Impacts of multiple stresses on water demand and supply across the Southeastern United States 1. JAWRA Journal of the American Water Resources Association 44 (6), 1441–1457.
Takele, G.S., Gebrie, G.S., Gebremariam, A.G., Engida, A.N., 2022. Future climate change and impacts on water resources in the Upper Blue Nile basin. J. Water Clim. Change 13 (2), 908–925. https://doi.org/10.2166/wcc.2021.235.
Taye, M.T., Dyer, E., Hirpa, F.A., Charles, K., 2018. Climate change impact on water resources in the Awash basin. Ethiopia. *Water (switzerland)* 10 (11), 1–16. https://doi.org/10.3390/w10111560.
Te Chow, V., Maidment, D. R., & Mays, L. W. (1988). *Applied hydrology*.
Teutschbein, C., Seibert, J., 2012. Bias correction of regional climate model simulations for hydrological climate-change impact studies: Review and evaluation of different methods. J. Hydrol. 456, 12–29.
UNEP. (1993). *World atlas of desertification: United Nations Environment Programme. London: Edward Arnold, 1992. 69 pp.* Pergamon.
Wang, K., Dickinson, R.E., 2012. A review of global terrestrial evapotranspiration: Observation, modeling, climatology, and climatic variability. Rev. Geophys. 50 (2) https://doi.org/10.1029/2011RG000373.
Weiß, M., Menzel, L., 2008. A global comparison of four potential evapotranspiration equations and their relevance to stream flow modelling in semi-arid environments. Adv. Geosci. 18, 15–23.
Worqlul, A.W., Dile, Y.T., Ayana, E.K., Jeong, J., Adem, A.A., Gerik, T., 2018. Impact of climate change on streamflow hydrology in headwater catchments of the Upper Blue Nile Basin. Ethiopia. *Water* 10 (2), 120.
Wyser, K., Van Noije, T., Yang, S., Von Hardenberg, J., O'Donnell, D., Döscher, R., 2020. On the increased climate sensitivity in the EC-Earth model from CMIP5 to CMIP6. Geosci. Model Dev. 13 (8), 3465–3474. https://doi.org/10.5194/gmd-13-3465-2020.
Yasarer, L.M.W., Sturm, B.S.M., 2016. Potential impacts of climate change on reservoir services and management approaches. Lake Reservoir Manage. 32 (1), 13–26. https://doi.org/10.1080/10402381.2015.1107665.